REVIEWS

Journal of Semiconductors
(2019) 40, 061003
doi: 10.1088/1674-4926/40/6/061003

Synthesis, properties, and applications of large-scale two-dimensional materials by polymer-assisted deposition

Hongtao Ren[1, 2], Yachao Liu[1], Lei Zhang[1, †], and Kai Liu[2, †]

[1]MOE Key Laboratory for Nonequilibrium Synthesis and Modulation of Condensed Matter, School of Science, Xi'an Jiaotong University, Xi'an 710049, China

[2]State Key Laboratory of New Ceramics and Fine Processing, School of Materials Science and Engineering, Tsinghua University, Beijing 100084, China

Abstract: Two-dimensional (2D) materials have attracted considerable attention because of their novel and tunable electronic, optical, ferromagnetic, and chemical properties. Compared to mechanical exfoliation and chemical vapor deposition, polymer-assisted deposition (PAD) is more suitable for mass production of 2D materials owing to its good reproducibility and reliability. In this review, we summarize the recent development of PAD on syntheses of 2D materials. First, we introduce principles and processing steps of PAD. Second, 2D materials, including graphene, MoS_2, and MoS_2/glassy-graphene heterostructures, are presented to illustrate the power of PAD and provide readers with the opportunity to assess the method. Last, we discuss the future prospects and challenges in this research field. This review provides a novel technique for preparing 2D layered materials and may inspire new applications of 2D layered materials.

Key words: polymer-assisted deposition; layered composite materials; glassy-graphene; MoS_2; heterostructures

Citation: H T Ren, Y C Liu, L Zhang, and K Liu, Synthesis, properties, and applications of large-scale two-dimensional materials by polymer-assisted deposition[J]. *J. Semicond.*, 2019, 40(6), 061003. http://doi.org/10.1088/1674-4926/40/6/061003

1. Introduction

Polymer-assisted deposition (PAD), which was first reported in 2004[1], provides a generalized strategy toward growing metal compounds with a desired chemical composition at low cost. Compared with other commonly used deposition methods such as physical vapor deposition (PVD)[2–4], and chemical vapor deposition (CVD)[4–7], PAD employs metal ions coordinated to polymers as the precursor. In PAD, the polymer has four notable features: (1) The formation of covalent complexes between the metal cations and the lone pair on the nitrogen atoms of the polymer enables the growth of thick or crack-free thin films. (2) The polymer precursor solution is highly stable in air for months. Additionally, the polymer maintains a homogeneous distribution of metal ions in the solution. Various metal–polymer solutions can be mixed at desired ratios. (3) The viscosity of the solution can be adjusted by simple removing water under vacuum or diluting with deionized water. (4) The polymer solution can be coated onto different substrates by using many methods, including spin, dip, spray, and inkjet coatings. More importantly, the conformal coating of porous materials[8–11] can be realized. In the past decades, metal oxides, metal nitrides, metal carbides, and two-dimensional (2D) layered materials have been successfully prepared by PAD as shown in Figs. 1 and 2.

The discovery of single-layer graphene via mechanical exfoliation in 2004[12] revealed that not only fabrication of stable, single-atom thick 2D materials from van der Waals solids is possible, but these materials exhibit extraordinary physical properties[13–15]. Their novel properties inspire many fundamental studies[16–19] and technological advancements[4, 20] for a wide range of applications including electronics, photonics, piezoelectrics, and spintronics. Mechanical exfoliation[19, 20] is a popular method for prototyping devices based on 2D materials. The main drawback of this method is that the size and productivity of materials and devices prepared are very limited. Another commonly used method for synthesizing high-quality 2D materials is chemical vapor deposition (CVD), which, however, is still not so cost-effective for syntheses of 2D materials. In contrast, PAD is a bottom-up, cost-effective, and precisely controlled method for large-scale production of 2D materials. In this review, we summarize the recent development of PAD particularly on syntheses of 2D materials. First, we introduce the principles and processing steps of PAD. Second, 2D materials, including graphene, MoS_2, and MoS_2/glassy-graphene heterostructures, are provided to illustrate the power of PAD and provide readers with the opportunity to assess the method. Last, we present the future prospects and challenges in this research field. This review provides a novel technique for preparing 2D materials and may inspire new applications of 2D materials.

2. Polymer-assisted deposition

2.1. Development of polymer-assisted deposition

The past 15 years have witnessed rapid developments in the preparation of epitaxial thin films by using PAD. Thus far, PAD has been successfully used to grow metal-oxides[21–24], metal-nitrides[11, 25–32], metal-carbides[33–35], single element materials (e.g., carbon films[9], Ge films[36], and glassy graphene[37, 38]), and TMD (MoS_2[16, 39, 40]) as shown in Figs. 1 and 2. In the past,

Correspondence to: L Zhang, zhangleio@xjtu.edu.cn; K Liu, liuk@tsinghua.edu.cn

Received 31 MARCH 2019; Revised 29 APRIL 2019.

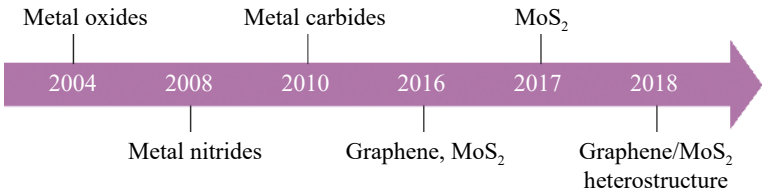

Fig. 1. (Color online) Timeline showing key development by polymer-assisted deposition. Metal oxides; metal nitrides; metal carbides; glassy-graphene; MoS_2; MoS_2/glassy-graphene heterostructure.

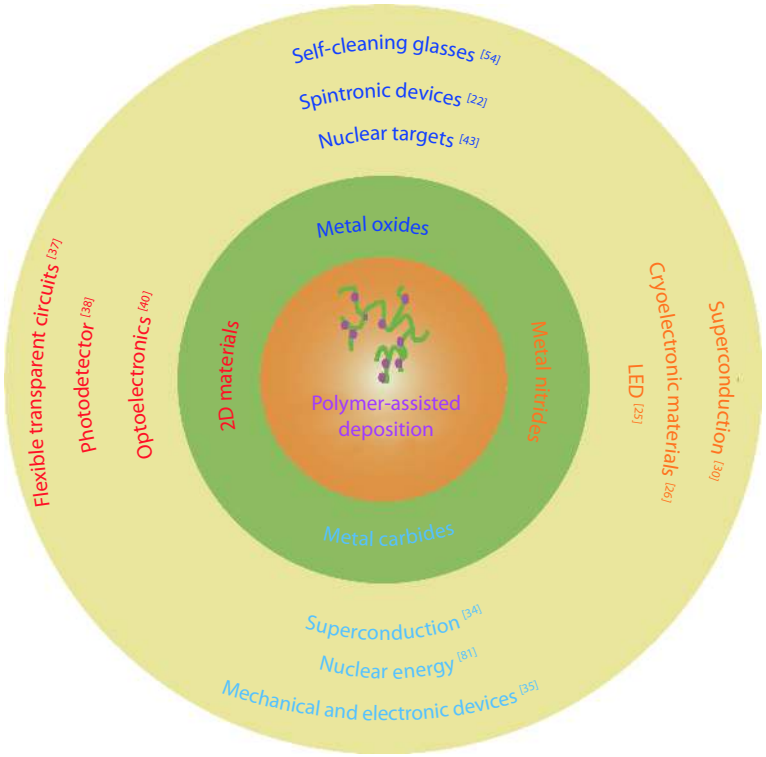

Fig. 2. (Color online) Application of as-grown thin films by PAD.

we built ZnO nanostructures[22–24]and MoS_2[16] thin films.

Metal oxides have received considerable attention because of their potential applications in nuclear targets[41–47], spintronic devices[22–24, 48–53], and self-cleaning glasses[54] due to their versatile properties, including ferroelectricity, ferromagnetism, piezoelectricity, semiconductivity, and superconductivity. Many simple oxides, such as Eu_2O_3[41–44], ZnO[21–24], TiO_2[1, 54–58], and VO_2[59–64] have been prepared by using PAD. Polymers can prevent metal ions from engaging in unwanted chemical reactions; thus, the growth of complex metal-oxide films through PAD is controllable and reproducible. Many complex metal-oxide thin films, such as $Ba_{1-x}Sr_xTiO_3$[50, 52, 65–67], $CuAlO_2$[68], mixed-valence perovskite[66], $BiVO_4$[69], $LiMn_2O_4$[70], $NiCo_2O_4$[71], Gd-CeO_2[72], $CuScO_2$[73], $CaCu_3Ti_4O_{12}$[74, 75], Re_2NiMnO_6[76], Co-$NdNiO_3$[77], $CuSc_{1-x}Sn_xO_2$[78], $Sm_{0.2}Ce_{0.8}O_{1.9-x}$[79], and $Y_3Fe_5O_{12}$[80], have been grown by using PAD.

Metal nitrides are used in many fields due to their hardness, electronic properties[11, 25–28, 32], superconductivity[26, 29–31], and magnetic properties[26, 31]. However, large mismatches exist in either the lattice parameters or the thermal expansion coefficients between the film and the substrate, contributing to great challenges in growth of epitaxial nitride films. In 2008, epitaxial GaN[25] thin films were deposited on (0001) sapphire substrates by PAD for the first time. PAD has also been used for growing binary nitride films, such as NbN[26], TiN[28], AlN[28, 32], MoN[29–31], and UN_2[81]. Complex metal nitride films, including $Ti_{1-x}Al_xN$[28], $BaZrN_2$[11], $BaHfN_2$[11], and $SrTiN_2$[27], have been deposited by using PAD.

Transition-metal carbides exhibit high melting point, high electrical conductivity[33, 35, 82], excellent mechanical properties[33–35], and good chemical resistance[81]. These properties make them desirable for applications in wear coatings, passivation layers, turbine engines, and aircraft. The growth of single elements (e.g., C[9] and Ge[36]) and carbides (e.g., TiC, NbC, VC, TaC, and UC_2)[33–35, 82, 83] has also been realized by using PAD.

Two-dimensional layered materials, such as graphene and MoS_2, are another type of materials prepared by PAD. In the past few years, glassy graphene[37], and MoS_2[16, 39, 40] thin films have been successfully obtained by PAD. In addition, 2D layered materials have been fabricated into various electronic devices.

2.2. Principles and processing steps of PAD

In the PAD process, metal ions are coordinated to the polymer as the precursor. Covalent complexes are formed between the metal cations and the lone pair on the nitrogen atoms of the polymer. Thus, the oligomerization reaction will

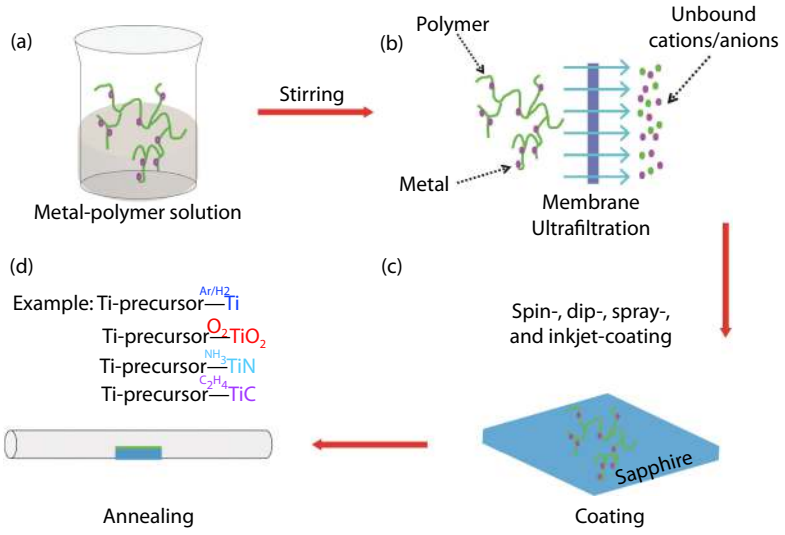

Fig. 3. (Color online) Schematic illustration of the main processing steps used to grow thin films by PAD.

Table 1. Elements in the magenta boxes coordinated with polymer to form a stable complex. The elements shown in red font were bound with the polymer in the previous reports.

I A																VIII A
H	II A											III A	IV A	V A	VI A	VII A	He
Li	Be											B	C	N	O	F	Ne
Na	Mg	III B	IV B	V B	VI B	VII B		VIII B		I B	II B	Al	Si	P	S	Cl	Ar
K	Ca	Sc	Ti	V	Cr	Mn	Fe	Co	Ni	Cu	Zn	Ga	Ge	As	Se	Br	Kr
Rb	Sr	Y	Zr	Nb	Mo	Tc	Ru	Rh	Rd	Ag	Cd	In	Sn	Sb	Te	I	Xe
Cs	Ba	La—Lu	Hf	Ta	W	Re	Os	Ir	Pt	Au	Hg	Tl	Pb	Bi	Po	At	Rn
Fr	Ra	Ac—Lr	Rf	Db	Sg	Bh	Hs	Mt	Ds	Rg	Cn						

La	Ce	Pr	Nd	Pm	Sm	Eu	Gd	Tb	Dy	Ho	Er	Tm	Yb	Lu
Ac	Th	Pa	U	Np	Pu	Am	Cm	Bk	Cf	Es	Fm	Md	No	Lr

not occur unless certain conditions are satisfied. Hence, the solutions are stable for months. At approximately 450 to 500 °C, the polyethyleneimine (PEI) polymer undergoes thermal depolymerization back to $NH_2CH=CH_2$. The ethylenediaminetetra-acetic acid (EDTA) decomposes to acetic acid, formic acid, and ethylenediamine even in inert or H_2 atmospheres.

The main processing steps involve the preparation of the metal-precursor solution, ultrafiltration, coating, and annealing. Fig. 3 illustrates the typical PAD steps for the growth of thin films. We will describe the unique chemistry and basic steps of PAD in the following part.

2.2.1. Preparation of metal-polymer solution

Table 1 summarizes over 45 different elements that can be coordinated with polymers to form a stable polymer precursor solution. In PAD, the polymer in the solution binds to the metal ions via electrostatic attraction, hydrogen bonding, and/or covalent bonding. The first-row transition metals, using nitrates, acetates or chlorides, bind easily to the simple PEI polymer. Other hard-to-bind metals, such as Sn^{2+} and Ti^{2+}, need the PEI to be functionalized with carboxylic acids to provide a stable coordination environment. The third method for binding metals utilizes the ability of protonated PEI to coordinate anionic metal complexes. For instance, EDTA could form stable complexes with almost all metals, and then the complexes successfully bind to the PEI.

In Table 2, we summarize 40 different elements that bind well to the polymer. These metal-polymer solutions have been reported in previous works. Interestingly, one metal elemental may be bound with different polymers (PEI or PEI-EDTA).

2.2.2. Ultrafiltration

The metal-polymer solution passes through a filter or membrane to remove cations and anions that are not coordinated polymers, as shown in Fig. 3(b). In the ultrafiltration process, Amicon® ultra centrifugal filtration units and a centrifugal apparatus are used for filtration in our experiments.

2.2.3. Coating

After ultrafiltration, the polymer solution is coated onto different conformation substrates via various methods, includ-

Table 2. Summary of various metal elements binded by polymers.

Element	Metal precursor	Polymer	Element	Metal precursor	Polymer
Li[70]	$LiNO_3$	PEI + EDTA	Ru[49]	$RuCl_3$	PAA
C[37]	$C_6H_{12}O_6$	PEI	Ag[84]	$AgNO_3$	PEI + $C_6H_8O_7$
Al[68]	$Al(NO_3)_3$	PEI + HF	In[85]	$In(NO_3)_3$	PEI
Ca[45]	$Ca(OH)_2$	PEI	Sn[86]	$SnCl_2$	PEIC
Sc[73]	$Sc(NO_3)_3$	PEI + EDTA	Ba[65]	$Ba(NO_3)_2$	PEI + EDTA
Ti[1]	$Ti(cat)_3(NH_4)_2$	PEI	Hf[42]	$HfCl_4$	PEI
V [10]	$VOSO_4$	PEI + EDTA	Ta[33]	$TaCl_5$	PEI + HF
Mn[45]	$MnCl_2$	PEI + EDTA	W[87]	$(NH_4)_2WO_4$	PEI
Fe[88]	$FeCl_3$	PEI	Bi[10]	$Bi(NO_3)_3$	PEI + EDTA
Co[88]	$CoCl_2$	PEI	La[45]	$La(NO_3)_3$	PEI + EDTA
Ni[51]	$Ni(NO_3)_2$	PEI + EDTA	Ce[72]	$Ce(NO_3)_3$	PEI + EDTA
Cu[68]	$Cu(NO_3)_2$	PEI	Pr[76]	$Pr(NO_3)_3$	PEI + EDTA
Zn[22]	$Zn(NO_3)_2$	PEI	Nd[76]	$Nd(NO_3)_3$	PEI + EDTA
Ga[25]	$GaCl_5$	PEI	Sm[76]	$Sm(NO_3)_3$	PEI + EDTA
Ge[36]	GeO_2	PEI + EDTA	Eu[42]	$EuCl_3$	PEI
Sr[1]	$Sr(NO_3)_2$	PEI + EDTA	Gd[72]	$Gd(NO_3)_3$	PEI + EDTA
Y[10]	$Y(NO_3)_3$	PEI + EDTA	Tm[42]	$TmCl_3$	PEI
Zr[55]	$ZrO(NO_3)_2$	PEI + EDTA	U[89]	$UO_2(oAc)_2$	PEI
Nb[26]	$NbCl_5$	PEI + HF	Np[46]	^{239}Np solution	PEI + EDTA
Mo[16]	$(NH_4)_6Mo_7O_{24}$	PEI + EDTA	Pu[46]	^{239}Pu solution	PEI + EDTA

ing spin, dip, spray, and inkjet. Therefore, the substrate need not to be flat, such as Anodisc™ membranes[10, 55], the grating coupler[56], carbon nanotubes (CNT), and quartz fibers[9, 35]. Furthermore, conformal coating and nanostructured materials may be realized successfully by PAD. This feature makes PAD attractive for use to grow the thin films, form the conformal coating, and synthesize the nanostructured materials.

2.2.4. Thermal de-polymerization and crystallization

To depolymerize the polymer and enable the crystallization of the film, the coated substrate is then treated in a controlled environment at the desired temperature. The water is driven out at moderate temperature (approximately 120 °C). Furthermore, the PAD process involves high -temperature (approximately 500 °C) exposure in a controlled environment to remove the polymer. The PEI and EDTA in the precursor film do not undergo combustion, but rather thermal depolymerization back to $NH_2CH=CH_2$, acetic acid, formic acid, and ethylenediamine. Notably, this non-combustive process can lead to reduced carbon contamination in the synthesized thin films.

The thin films may be single-crystal, polycrystalline, or amorphous, depending on the annealing temperature and substrate used. Importantly, the composition of as-grown materials is determined by the metal precursor, temperature, and atmospheric environment. For example: (1) the thermal treatment of the precursor film containing Ti ions in a reducing atmosphere, such as argon mixed with hydrogen, will result in pure Ti. (2) the precursor film will be converted to TiO_2 if the thermal treatment is performed in pure oxygen[1, 11, 43, 90, 91]; (3) the same precursor film will be transformed to TiN, if the thermal treatment is carried out in an ammonia atmosphere[42]; and (4) the precursor film will be converted to TiC if the thermal treatment is carried out in a gas mixture of ethylene and forming gas (Ar with H_2)[33, 35]. Furthermore, high-quality epitaxial films have been grown using PAD by using a lattice matched substrate and optimal temperature profiles.

3. Large-scale 2D materials by PAD

3.1. Transparent carbon films and glassy graphene thin films

Transparent conducting films are highly important to electronic, flexible, and transparent devices. Graphene has potential applications in solar cells, touch panels, wearable electronics, and flexible displays[37, 38]. To prepare graphene or carbon thin films, various precursors have been used as carbon sources. In addition, graphitic carbon and glassy graphene have been successfully fabricated via PAD[9, 37]. Furthermore, previous experimental results show that it is possible to fabricate large-scale heterostructures.

Cao *et al.*[9]. utilized PEI as a carbon source for depositing transparent carbon film on different quartz substrates. In this work, Cu ions are first introduced to grow the graphitic carbon. Further, introducing Cu ions could not only improve the decomposition temperature of PEI, but also help the graphitization of the carbon thin film. Finally, the Cu nanoparticles are removed by immersing the film into $FeCl_3$ solutions and etching Cu to keep the carbon film unbroken. The partially graphitized transparent carbon film is deposited by the PAD of the Cu^{2+} coordinated PEI.

As shown in Figs. 4 and 5, glucose ($C_6H_{12}O_6$) was utilized by Dai *et al.*[37] as a carbon source for depositing ultra-smooth glassy graphene thin films.

The three types of carbon-based thin films are deposited by PAD under different catalysis conditions, as shown in Fig. 4. (1) The glassy carbon film, which is partially crystallized and disordered, is grown in Figs. 4(a)–4(c). (2) Glassy graphene, an intermediate state between glassy carbon and graphene, is obtained at 850 °C as shown in Fig. 4(d). TEM studies in Fig. 4(f) show twisted lattice planes. The bent and curved lattice plane is one of the distinguishing features of glassy graphene. (3) When the annealing temperature is increased to 1000 °C, graphene evolves from glassy graphene. From the HRTEM lattice image and the six reflex spots in the SAED, we could con-

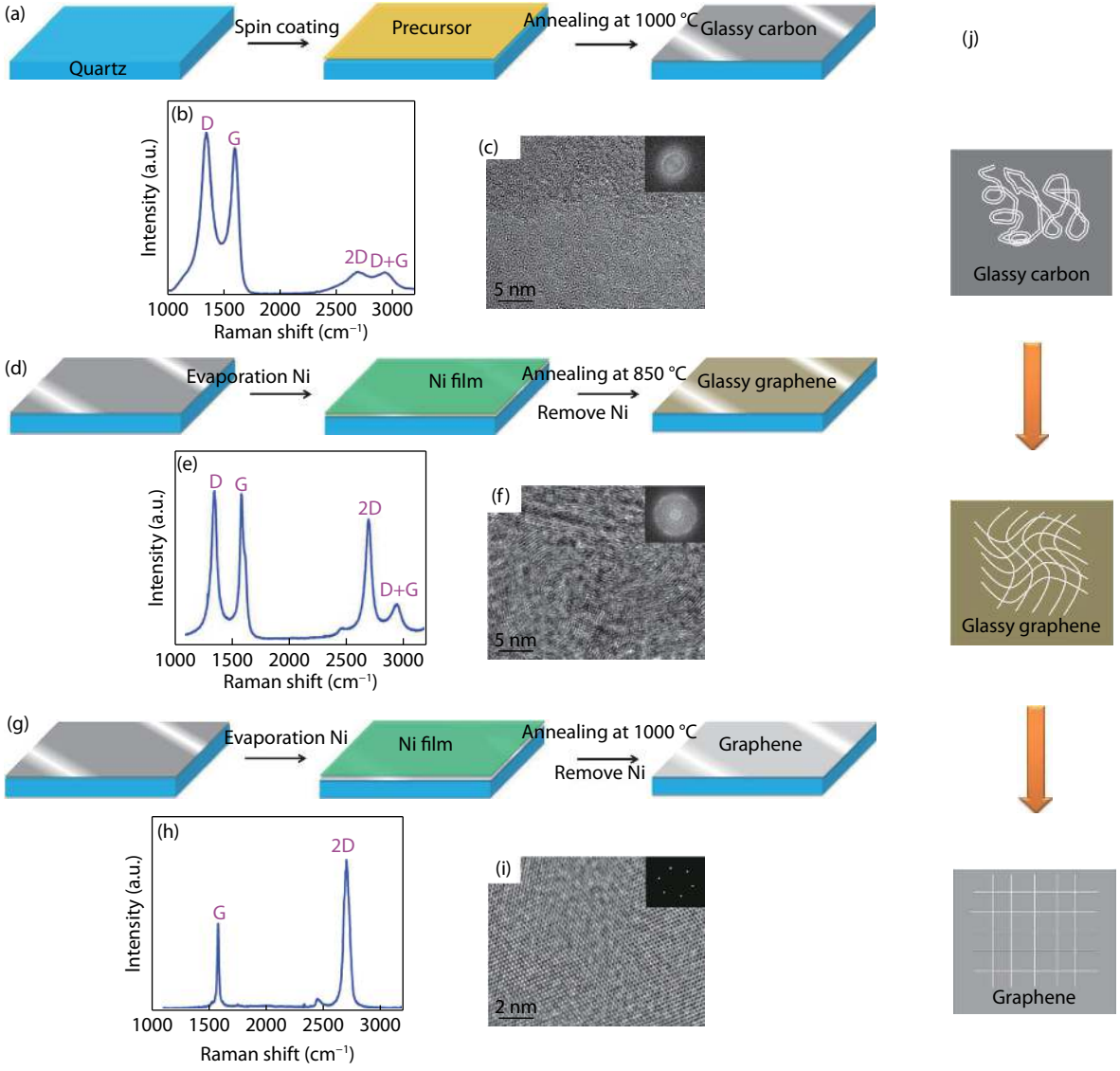

Fig. 4. (Color online) Evolution from glassy carbon to glassy-graphene and graphene[37].

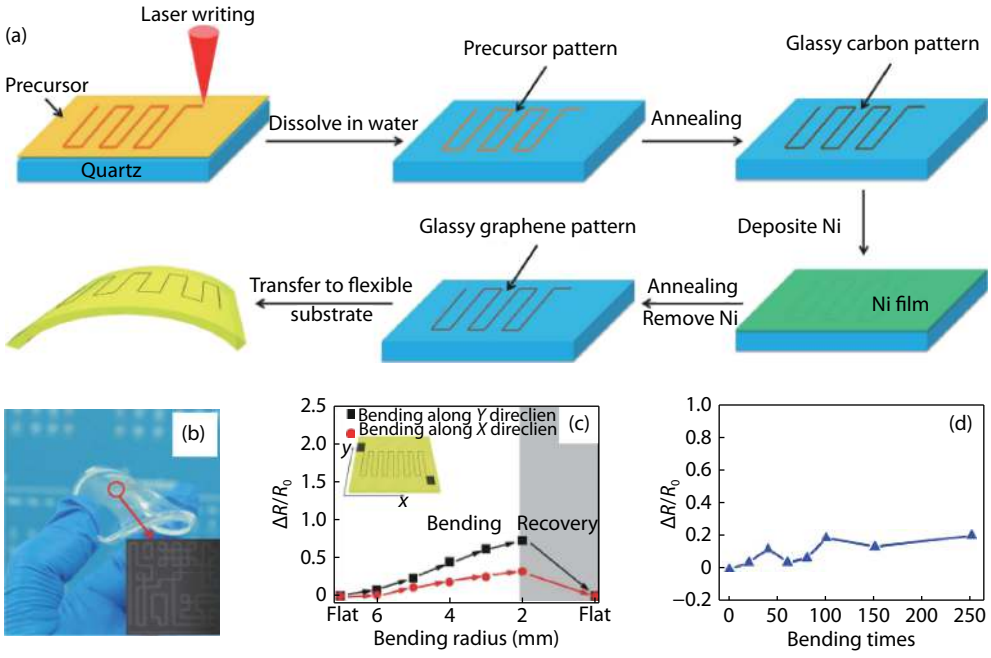

Fig. 5. (Color online) Preparation of glassy graphene-based circuits and the flexibility test[37].

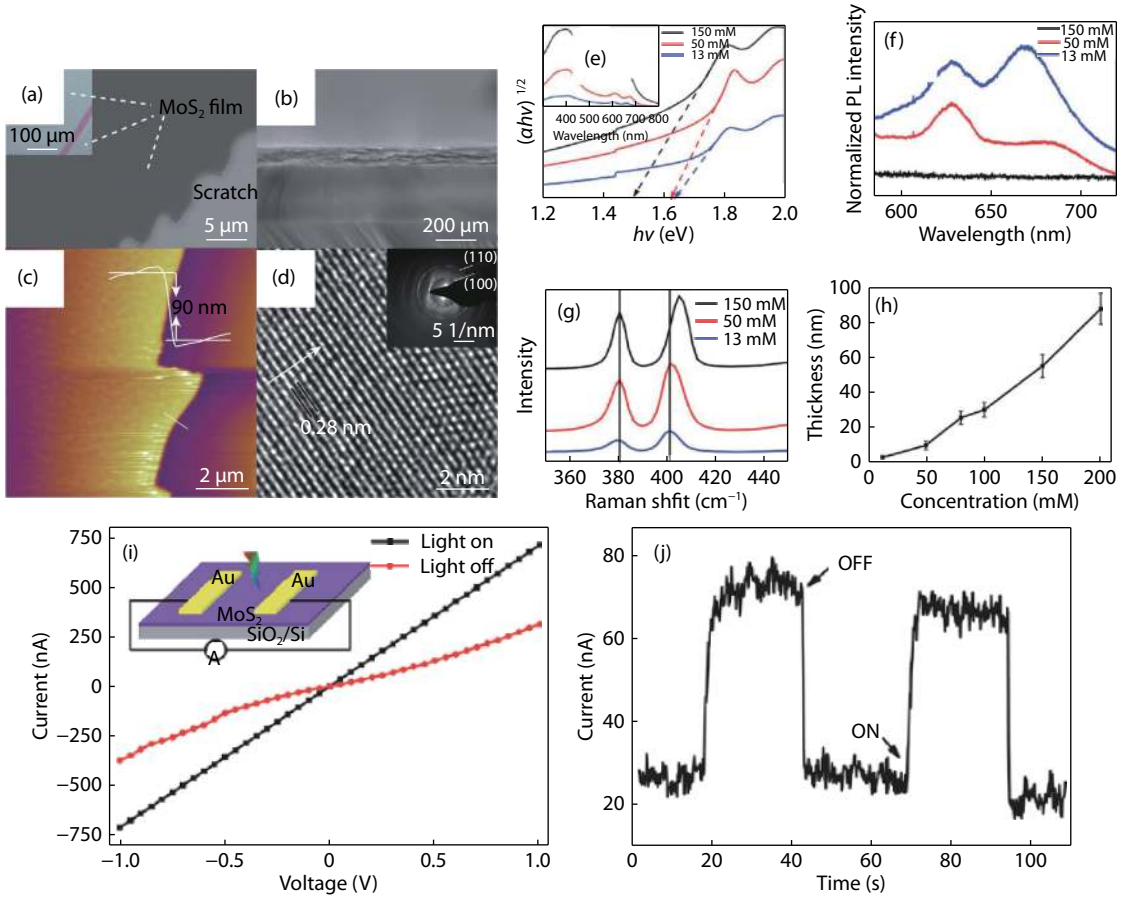

Fig. 6. (Color online) Thickness-dependent bandgap tunable MoS_2 thin films for optoelectronics[40].

firm the high-quality of graphene in Fig. 4(i). Based on the above analysis, the structural evolution of the three types of material is described in Fig. 4(j). In addition, glassy carbon is partially crystallized and disordered as shown in Fig. 4(c); the glassy graphene in Fig. 4(f) shows a high crystal quality but has twisted, bent lattice planes; and the graphene in Fig. 4(i) has perfect lattices.

Fig. 5(a) indicates that a circuit pattern is obtained after the laser writing and rinsing process. The glassy graphene circuits may be easily transferred to any substrate after annealing, as shown in Fig. 5(b), such as a flexible or rigid substrate. In Fig. 5(c), the sheet resistance is mediated with the bending radius. In addition, the vibration is anisotropic. After repeated bending or twisting, the resistance does not show any obvious changes as shown in Fig. 5(d). In this work, graphene FET is also fabricated to explore its potential application.

For the first time, an ultra-smooth glassy graphene thin film is grown by PAD at the inch scale. The thin film exhibits excellent conductivity, transparency, flexibility, and mechanical and chemical stability. Most importantly, as-deposited thin films are imprinted in flexible and transparent devices.

3.2. Highly scalable synthesis of MoS_2 thin films

Two-dimensional semiconductors MoS_2 are attracting a wide range of research interest due to their potential applications. MoS_2 thin films are also prepared through PAD. Furthermore, as-deposited thin films are fabricated into a photodetector with a broad spectral response and excellent performance.

Zhu *et al.*[40] reported growing thickness-controlled MoS_2 films by using PAD for the first time. In the PAD process, $(NH_4)_6Mo_7O_{24}{\cdot}4H_2O$ and pure sulfur serve as Mo and S sources, respectively. The thickness of the films adjusted by the precursor concentration can be readily changed from 50 to 2.5 nm.

Figs. 6(a)–6(d) shows that the thin film is smooth, continuous, homogeneous, and dense. The thickness and root-mean-square (RMS) surface roughness of the MoS_2 thin film are approximately 90 and 10.7 nm, respectively. The HRTEM image and the SAED pattern suggest that the film has high crystallinity.

In addition, the optical band gap energies for the films with different thicknesses are estimated by the UV–vis absorption spectra. The PL responses are the intensity decay and red-shifted in thicker films in Fig. 6(g). The A_{1g} peak shows a blue-shift, which is consistent with the previous report. Notably, the thickness is mediated by the concentration of the Mo precursor.

To explore their photoresponse properties, MoS_2 films are fabricated into photoconductors, and then characterized under simulated AM 1.2 illumination. Interestingly, the ratio of conductivity under illumination to dark conductivity is near 3, and the average response time is approximately 0.3 s, as shown in Table 3.

Yang *et al.*[39] developed a highly scalable coating process using PAD without sulfurization. The anhydrous ammonium tetrathiomolybdate (ATM) is converted into MoS_3 (120–260 °C) or 2H-MoS_2 (> 400 °C). The color difference with various thicknesses is shown in Fig. 7.

Large-scale and controllable thickness is the main characteristic of MoS_2 thin films from PAD. Given that most of as-grown

Table 3. Comparison of three different methods to synthesize MoS_2 and MoS_2 field-effect transistor structures.

Method	Precursor gas	Temperature (°C)	Crystalization	Conformal	Size	Mobility ($cm^2/(V·s)$)	Response time	I_{on}/I_{off} ratio
CVD	Ar	1000	Single-crystal	No	~cm^2	9.6	–	10^5[92]
	Ar	850	Single-crystal	No	–	50	–	10^6[92]
ALD	H_2S; Ar	60	Amorphous	Yes	–	0.23	–	10^2[93]
PAD	Ar + H_2	850	Polycrystalline	Yes	~cm^2	–	0.3 ms	3[40]
	Ar + H_2	700	Polycrystalline	Yes	6-inch	–	1.0 ms	10^4[39]
	Ar + H_2	550	Amorphous	Yes	~cm^2	–	–	–[16]

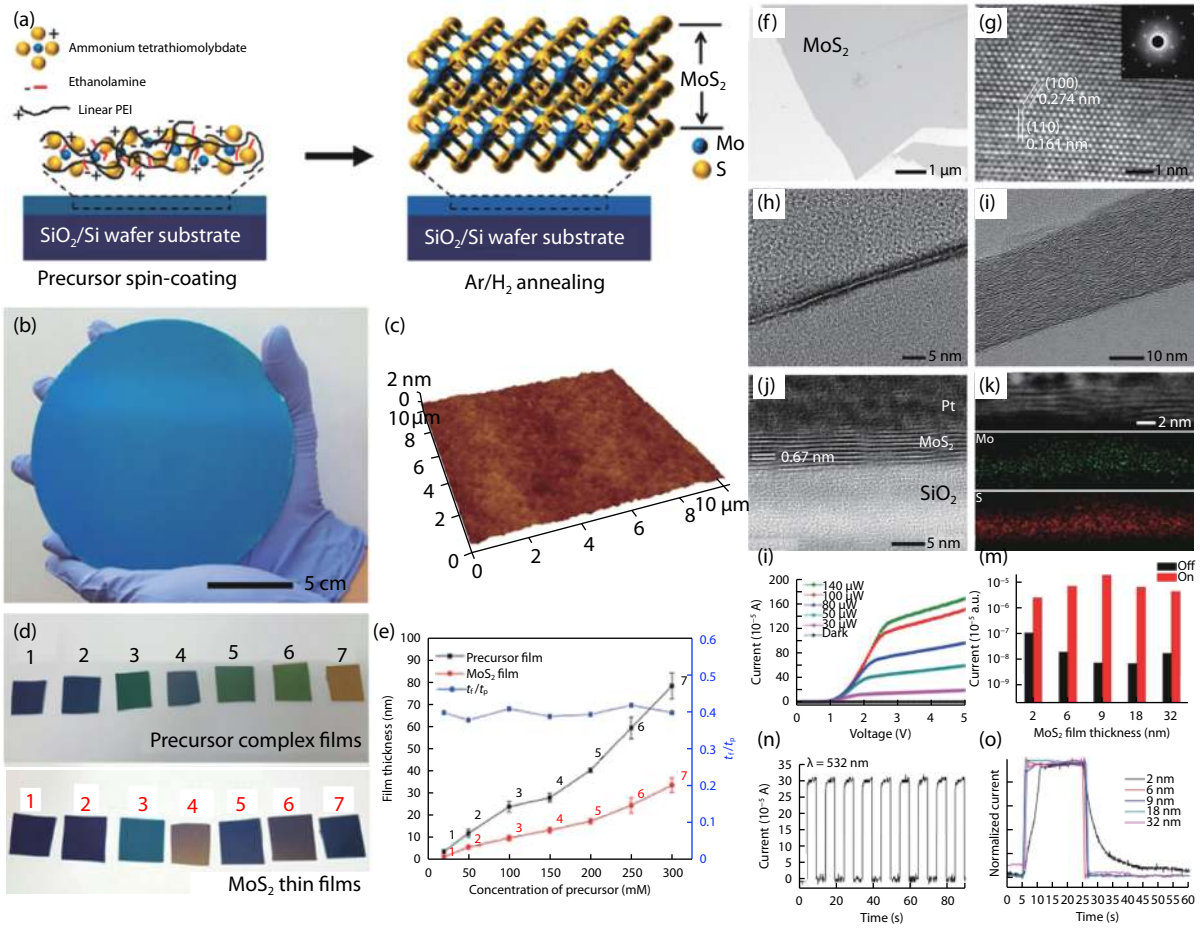

Fig. 7. (Color online) Wafer-scale synthesis of MoS_2 thin films via polymer-assisted deposition[39].

thin films are polycrystalline and have many defects, the photodetector fabricated by as-deposited MoS_2 thin films did not exhibit excellent properties, as shown in Table 3.

Ren *et al.*[16] employed MoS_2 thin films to study the dynamic propagation of web telephone-cord buckles, as shown in Fig. 8(a). Parts (b)–(g) of Fig. 8 show a point load applied by a probe that can initiate several branches of telephone-cord buckles. Subsequently, each cord front will branch into two new daughter cords after a certain distance of propagation, forming web buckles with many node positions. Furthermore, the 3D features of web buckles are probed by atomic force microscopy. Interestingly, the buckled semiconducting films have potential applications as diffusive reflection coatings, capillary microchannels, and hydrogen evolution reaction electrodes.

3.3. MoS_2/glassy-graphene heterostructures as transparent photodetectors

Based on the previous experiment results[37, 40], MoS_2/glassy-graphene heterostructures on quartz substrates have been successfully prepared using a vertically layer-stacking approach. The heterostructures synthesis procedure is illustrated. (1) The $MoS_2/SiO_2/Si$ nanosheet is spin coated with polymethyl-methacrylate (PMMA). (2) The PMMA/MoS_2 layer is separated from the SiO_2/Si substrate. (3) A g-graphene/quartz nanosheet is patterned by O_2 plasma etching. (4) The PMMA/MoS_2 is transferred onto the g-graphene/quartz, followed by the removal of PMMA and cleaning. As seen in Fig. 9(b), the heterostructures exhibit good transparency. The schematic of the transparent photodetector based on the MGH/quartz is shown in Fig. 9(c).

In summary, the heterostructures are synthesized by a layer-by-layer transfer technique, and their application as transparent photodetectors are reported for the first time[38].

4. Prospective and challenges

Compared with the experimental methods, such as chemical vapor deposition (CVD) and atomic layer deposition (ALD),

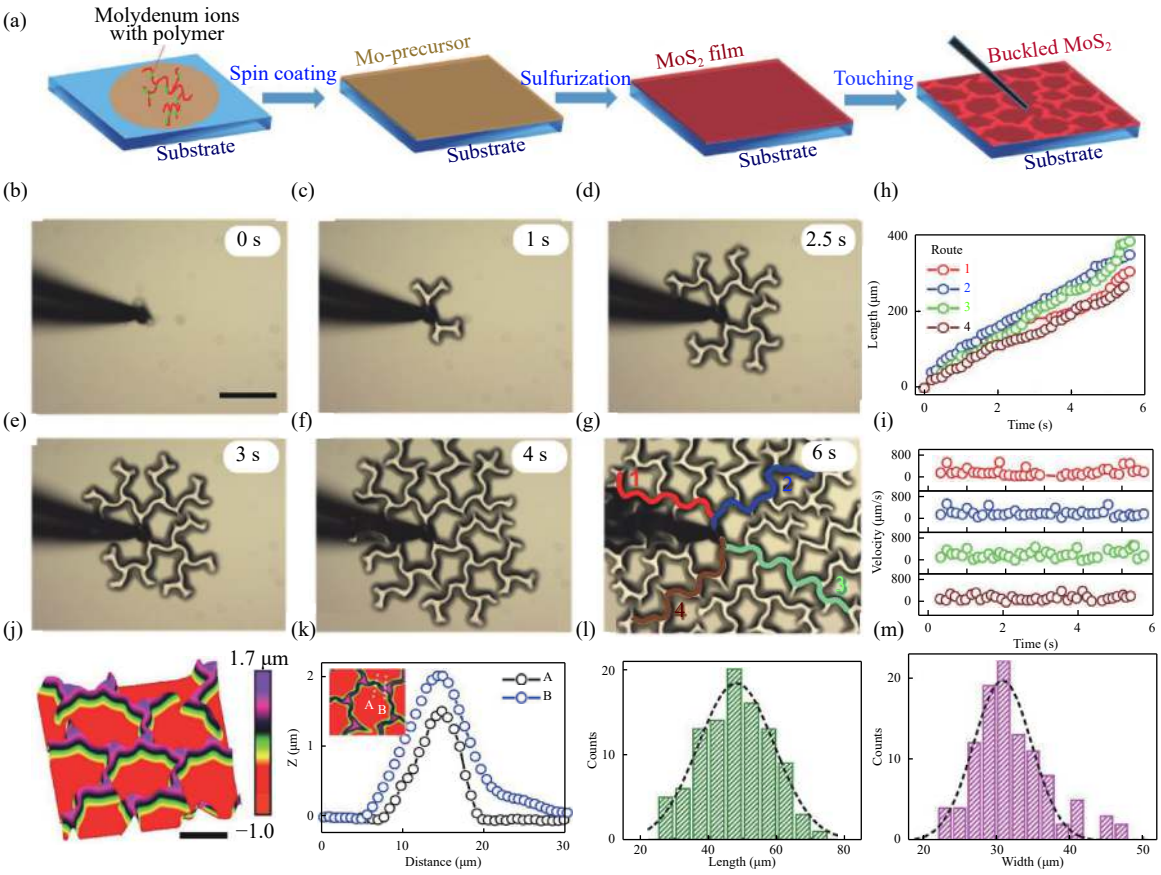

Fig. 8. (Color online) Formation of large-area web buckles[16].

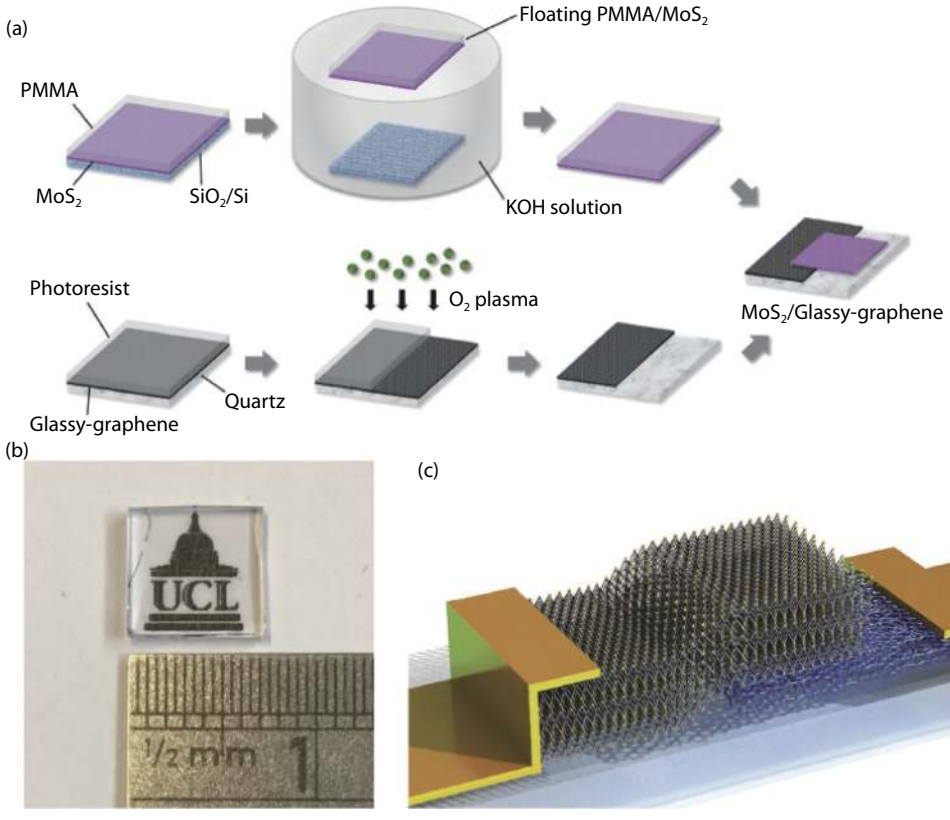

Fig. 9. (Color online) Schematic of MGH preparation and 3D view of the transparent photodetector, photoresponsivity and time-resolved photoresponse of photodetectors under different illuminations[38].

polymer-assisted deposition (PAD) has the advantages of low cost, large scale, easy doping and conformal coatings.

Some novel 2D semiconductors and various functional thin films have been successfully deposited by PAD, but it still remains several challenges on the synthesis of mono-layer thin films. Most of current MoS_2 thin films synthesized by PAD still have few layers and are polycrystalline with many defects. The growth of large-scale mono-layer thin films may be difficult to realize by PAD, thereby affecting the transport performance of the corresponding devices. In the future, if large single crystals can be realized by PAD, their device applications will be fully extended to mass production.

The other challenge is the preparation of 2D materials with doping by PAD. Doping, which is the intentional introduction of impurities into a parent material, plays a significant role in functionalizing 2D materials. For example, the wolfram and selenium chemical doping of MoS_2 is an effective way of engineering the optical bandgap[94], and Nb-, Co-, and Mn-doped MoS_2 few layers exhibit excellent transport properties[95]. Magnetic atoms, such as Mn, Fe, Co, and Ni, doped 2D TMDs, are promising as 2D diluted magnetic semiconductors, and have been predicted to exhibit ferromagnetic behavior at room temperature[96–98]. Thus far, most studies on doping of 2D materials have been intensively focused on the methods of mechanical exfoliation, CVD, and solvothermal methods, but few on PAD. The development of doping 2D semiconductors with novel properties by PAD is a promising research direction because they have various potential applications in optoelectronic, spintronics[100], hydrodeoxygenation reaction[99], and hydrogen evolution reaction[94].

As a characteristic of PAD, conformal coatings have been grown on non-planar surfaces such as quartz fibers[9, 35] in the past. Yi *et al.*[35] reported the synthesis of carbon nanotube/TiC hybrid fibers with improved mechanical strength and electrical conductivity. In this work, a dense and more compact fiber was formed. The transparent carbon film[9] was easily coated onto flexible quartz fiber by dip coating. The carbon thin film wrapped the quartz fiber tightly and uniformly, suggesting the excellent combination between carbon film and the quartz fiber.

Acknowledgments

L.Z. acknowledges support from the National Natural Science Foundation of China (Grant No.11774279), the Young Talent Support Plan of Xi'an Jiaotong University, and the Instrument Analysis Center of Xi'an Jiaotong University. K.L. acknowledges the support from National Key R&D Program of China (No. 2018YFA0208400), National Natural Science Foundation of China (Nos. 51602173 and 11774191), and Fok Ying-Tong Education Foundation (No. 161042).

References

[1] Jia Q X, McCleskey T M, Burrell A K, et al. Polymer-assisted deposition of metal-oxide films. Nat Mater, 2004, 3, 529

[2] Feng Q, Mao N, Wu J, et al. Growth of $MoS_{2(1-x)}Se_{2x}$ (x = 0.41–1.00) monolayer alloys with controlled morphology by physical vapor deposition. ACS Nano, 2015, 9(7), 7450

[3] Feng Q, Zhu Y, Hong J, et al. Growth of large-area 2D $MoS_{2(1-x)}$-Se_{2x} semiconductor alloys. Adv Mater, 2014, 26(17), 2648

[4] Hou J, Wang X, Fu D, et al. Modulating photoluminescence of monolayer molybdenum disulfide by metal-insulator phase transition in active substrates. Small, 2016, 12(29), 3976

[5] Kang K, Xie S, Huang L, et al. High-mobility three-atom-thick semiconducting films with wafer-scale homogeneity. Nature, 2015, 520, 656

[6] Dumcenco D, Ovchinnikov D, Marinov K, et al. Large-area epitaxial monolayer MoS_2. ACS Nano, 2015, 9(4), 4611

[7] Kochat V, Apte A, Hachtel J A, et al. Re doping in 2D transition metal dichalcogenides as a new route to tailor structural phases and induced magnetism. Adv Mater, 2017, 29(43), 1703754

[8] Shukla P, Lin Y, Minogue E M, et al. Polymer assisted deposition (PAD) of thin metal films: A new technique to the preparation of metal oxides and reduced metal films. Actinides 2005-Basic Science, Applications and Technology, 2006, 893

[9] Cao Y, Dai X, Zhang K, et al. One-step aqueous solution route toward depositing transparent carbon film onto different quartize substrate. Mater Lett, 2016, 185, 135

[10] Bauer E, Mueller A H, Usov I, et al. Chemical solution route to conformal phosphor coatings on nanostructures. Adv Mater, 2008, 20(24), 4704

[11] Luo H, Wang H, Bi Z, et al. Highly conductive films of layered ternary transition-metal nitrides. Angew Chem Int Edit, 2009, 48(8), 1490

[12] Novoselov K S, Geim A K, Morozov S V, et al. Electric field effect in atomically thin carbon films. Science, 2004, 306(5696), 666

[13] Liu K, Wu J. Mechanical properties of two-dimensional materials and heterostructures. J Mater Res, 2015, 31(7), 832

[14] Sun Y, Wang R, Liu K. Substrate induced changes in atomically thin 2-dimensional semiconductors: fundamentals, engineering, and applications. Appl Phys Rev, 2017, 4(1), 011301

[15] Yuan Z, Hou J, Liu K. Interfacing 2D semiconductors with functional oxides: fundamentals, properties, and applications. Crystals, 2017, 7(9), 265

[16] Ren H, Xiong Z, Wang E, et al. Watching dynamic self-assembly of web buckles in strained MoS_2 thin films. ACS Nano, 2019, 13, 3106

[17] Sun Y, Liu K. Strain engineering in functional 2-dimensional materials. J Appl Phys, 2019, 125(8), 082402

[18] Sun Y, Pan J, Zhang Z, et al. Elastic properties and fracture behaviors of biaxially deformed, polymorphic $MoTe_2$. Nano Lett, 2019, 19(2), 761

[19] Wang X, Fan W, Fan Z, et al. Substrate modified thermal stability of mono- and few-layer MoS_2. Nanoscale, 2018, 10(7), 3540

[20] Hong S, Fu D, Hou J, et al. Robust photoluminescence energy of MoS_2/graphene heterostructure against electron irradiation. Sci China Mater, 2018, 61(2095–8226), 1351

[21] Lin Y, Xie J, Wang H, et al. Green luminescent zinc oxide films prepared by polymer-assisted deposition with rapid thermal process. Thin Solid Films, 2005, 492(1/2), 101

[22] Ren H, Xiang G, Gu G, et al. Zinc vacancy-induced room-temperature ferromagnetism in undoped ZnO thin films. J Nanomater, 2012, 6, 295358

[23] Ren H, Xiang G, Gu G, et al. Enhancement of ferromagnetism of ZnO:Co nanocrystals by post-annealing treatment: The role of oxygen interstitials and zinc vacancies. Mater Lett, 2014, 122, 256

[24] Ren H, Xiang G, Luo J, et al. Direct catalyst-free self-assembly of large area of horizontal ferromagnetic ZnO nanowire arrays. Mater Lett, 2019, 234, 384

[25] Luo H, Lin Y, Wang H, et al. Epitaxial GaN thin films prepared by polymer-assisted deposition. J Phys Chem C, 2008, 112(51), 20535

[26] Zou G, Jain M, Zhou H, et al. Ultrathin epitaxial superconducting niobium nitride films grown by a chemical solution technique. Chem Commun, 2008(45), 6022

[27] Luo H, Wang H, Bi Z, et al. Epitaxial ternary nitride thin films pre-

pared by a chemical solution method. J Am Chem Soc, 2008, 130(46), 15224
[28] Luo H, Lin Y, Wang H, et al. A chemical solution approach to epitaxial metal nitride thin films. Adv Mater, 2009, 21(2), 193
[29] Luo H, Zou G, Wang H, et al. Controlling crystal structure and oxidation state in molybdenum nitrides through epitaxial stabilization. J Phys Chem C, 2011, 115(36), 17880
[30] Zhang Y, Haberkorn N, Ronning F, et al. Epitaxial superconducting delta-MoN films grown by a chemical solution method. J Am Chem Soc, 2011, 133(51), 20735
[31] Haberkorn N, Zhang Y Y, Kim J, et al. Upper critical magnetic field and vortex-free state in very thin epitaxial delta-MoN films grown by polymer-assisted deposition. Supercond Sci Tech, 2013, 26(10), 105023
[32] Pan T S, Zhang Y, Huang J, et al. Particle size effect on thermal conductivity of AlN films with embedded diamond particles. Appl Phys A, 2014, 114(3), 973
[33] Zou G, Wang H, Mara N, et al. Chemical solution deposition of epitaxial carbide films. J Am Chem Soc, 2010, 132(8), 2516
[34] Zou G, Luo H, Zhang Y, et al. A chemical solution approach for superconducting and hard epitaxial NbC film. Chem Commun, 2010, 46(41), 7837
[35] Yi Q, Dai X, Zhao J, et al. Enhanced mechanical strength and electrical conductivity of carbon-nanotube/TiC hybrid fibers. Nanoscale, 2013, 5(15), 6923
[36] Zou G F, Luo H M, Ronning F, et al. Facile chemical solution deposition of high-mobility epitaxial germanium films on silicon. Angew Chem Int Edit, 2010, 49(10), 1782
[37] Dai X, Wu J, Qian Z, et al. Ultra-smooth glassy graphene thin films for flexible transparent circuits. Sci Adv, 2016, 2(11), e1601574
[38] Xu H, Han X, Dai X, et al. High detectivity and transparent few-layer MoS_2/glassy-graphene heterostructure photodetectors. Adv Mater, 2018, 30(13), e1706561
[39] Yang H, Giri A, Moon S, et al. Highly scalable synthesis of MoS_2 thin films with precise thickness control via polymer-assisted deposition. Chem Mater, 2017, 29(14), 5772
[40] Zhu J T, Wu J, Sun Y H, et al. Thickness-dependent bandgap tunable molybdenum disulfide films for optoelectronics. Rsc Adv, 2016, 6(112), 110604
[41] Lin Y, Wang H, Hawley M E, et al. Epitaxial growth of Eu_2O_3 thin films on $LaAlO_3$ substrates by polymer-assisted deposition. Appl Phys Lett, 2004, 85(16), 3426
[42] Garcia M A, Ali M N, Parsons-Moss T, et al. Metal oxide films produced by polymer-assisted deposition (PAD) for nuclear science applications. Thin Solid Films, 2008, 516(18), 6261
[43] Ali M N, Garcia M A, Parsons-Moss T, et al. Polymer-assisted deposition of homogeneous metal oxide films to produce nuclear targets. Nat Protoc, 2010, 5(8), 1440
[44] Garcia M A, Ali M N, Chang N N, et al. Metal oxide targets produced by the polymer-assisted deposition method. Nucl Instrum Meth A, 2010, 613(3), 396
[45] Jain M, Shukla P, Li Y, et al. Manipulating magnetoresistance near room temperature in $La_{0.67}Sr_{0.33}MnO_3$/$La_{0.67}Ca_{0.33}MnO_3$ films prepared by polymer assisted deposition. Adv Mater, 2006, 18(20), 2695
[46] McCleskey T M, Bauer E, Jia Q, et al. Optical band gap of NpO_2 and PuO_2 from optical absorbance of epitaxial films. J Appl Phys, 2013, 113(1), 013515
[47] Wen X D, Loeble M W, Batista E R, et al. Electronic structure and O K-edge XAS spectroscopy of U_3O_8. J Electron Spectrosc, 2014, 194, 81
[48] Jain M, Li Y, Hundley M F, et al. Magnetoresistance in polymer-assisted deposited Sr- and Ca-doped lanthanum manganite films. Appl Phys Lett, 2006, 88(23), 232510
[49] Luo H M, Jain M, Baily S A, et al. Structural and ferromagnetic properties of epitaxial $SrRuO_3$ thin films obtained by polymer-assisted deposition. J Phys Chem B, 2007, 111(26), 7497
[50] Jain M, Lin Y, Shukla P, et al. Ferroic metal-oxide films grown by polymer assisted deposition. Thin Solid Films, 2007, 515(16), 6411
[51] Luo H, Yang H, Bally S A, et al. Self-assembled epitaxial nanocomposite $BaTiO_3$–$NiFe_2O_4$ films prepared by polymer-assisted deposition. J Am Chem Soc, 2007, 129(46), 14132
[52] Jain M, Bauer E, Lin Y, et al. $BaTiO_3$-related ferroelectric thin fflms by polymer assisted deposition. Integr Ferroelectr, 2008, 100, 132
[53] Lucas I, Vila-Fungueirino J M, Jimenez-Cavero P, et al. Tunnel conduction in epitaxial bilayers of ferromagnetic $LaCoO_3$/$La_{2/3}Sr_{1/3}MnO_3$ deposited by a chemical solution method. ACS Appl Mater Inter, 2014, 6(23), 21279
[54] Yi Q, Wang H, Cong S, et al. Self-cleaning glass of photocatalytic anatase TiO_2@carbon nanotubes thin film by polymer-assisted approach. Nanoscale Res Lett, 2016, 11, 457
[55] Shukla P, Minogue E M, McCleskey T M, et al. Conformal coating of nanoscale features of microporous Anodisc™ membranes with zirconium and titanium oxides. Chem Commun, 2006(8), 847
[56] Gillman E S, Costello D, Moreno M, et al. Polymer-assisted conformal coating of TiO_2 thin films. J Appl Phys, 2010, 108(4), 044310
[57] Lin Y, Zeng B, Ji Y, et al. Nucleation dynamics of nanostructural TiO_2 films with controllable phases on (001) $LaAlO_3$. Nanotechnology, 2014, 25(1), 014014
[58] Yi Q H, Cong S, Wang H, et al. High-stability Ti^{4+} precursor for the TiO_2 compact layer of dye-sensitized solar cells. Appl Surf Sci, 2015, 356, 587
[59] Ji Y, Zhang Y, Gao M, et al. Role of microstructures on the M_1–M_2 phase transition in epitaxial VO_2 thin films. Sci Rep-UK, 2014, 4, 4854
[60] Ji Y, Zhang Y, Gao M, et al. Growth and physical properties of vanadium oxide thin films with controllable phases. MRS Proceedings, 2013, 1547, 21
[61] Yue F, Huang W, Shi Q, et al. Phase transition properties of vanadium oxide films deposited by polymer-assisted deposition. J Sol-Gel Sci Techn, 2014, 72(3), 565
[62] Breckenfeld E, Kim H, Gorzkowski E P, et al. Laser-processing of VO_2 thin films synthesized by polymer-assisted-deposition. Appl Surf Sci, 2017, 397, 152
[63] Gao M, Qi Z, Lu C, et al. Interplay between extra charge injection and lattice evolution in VO_2/CH_3NH_3 PbI_3 heterostructure. Phys Status Solidi R, 2018, 1700416
[64] Liang W, Gao M, Lu C, et al. Enhanced metal-insulator transition performance in scalable vanadium dioxide thin films prepared using a moisture-assisted chemical solution approach. ACS Appl Mater Inter, 2018, 10(9), 8341
[65] Lin Y, Lee J S, Wang H, et al. Structural and dielectric properties of epitaxial $Ba_{1-x}Sr_xTiO_3$ films grown on $LaAlO_3$ substrates by polymer-assisted deposition. Appl Phys Lett, 2004, 85(21), 5007
[66] Jain M, Bauer E, Ronning F, et al. Mixed-valence perovskite thin films by polymer-assisted deposition. J Am Ceram Soc, 2008, 91(6), 1858
[67] Yao G, Ji Y, Liang W, et al. Influence of the vicinal surface on the anisotropic dielectric properties of highly epitaxial $Ba_{0.7}Sr_{0.3}TiO_3$ thin films. Nanoscale, 2017, 9(9), 3068
[68] Luo H, Jain M, McCleskey T M, et al. Optical and structural properties of single phase epitaxial p-type transparent oxide thin films. Adv Mater, 2007, 19(21), 3604
[69] Luo H, Mueller A H, McCleskey T M, et al. Structural and photoelectrochemical properties of $BiVO_4$ thin films. J Phys Chem C, 2008, 112(15), 6099
[70] Xu Y, Chen G, Fu E, et al. Nickel substituted $LiMn_2O_4$ cathode

with durable high-rate capability for Li-ion batteries. Rsc Adv, 2013, 3(40), 18441

[71] Yuan C Z, Li J Y, Hou L R, et al. Polymer-assisted synthesis of a 3D hierarchical porous network-like spinel $NiCo_2O_4$ framework towards high-performance electrochemical capacitors. J Mater Chem A, 2013, 1(37), 11145

[72] Mos R B, Petrisor T Jr, Nasui M, et al. Enhanced structural and morphological properties of Gd-doped CeO_2 thin films obtained by polymer-assisted deposition. Mater Lett, 2014, 124, 306

[73] Chuai Y H, Shen H Z, Li Y, et al. Epitaxial growth of highly infrared-transparent and conductive $CuScO_2$ thin film by polymer-assisted-deposition method. Rsc Adv, 2015, 5(61), 49301

[74] Lin Y, Feng D Y, Gao M, et al. Reducing dielectric loss in $CaCu_3Ti_4O_{12}$ thin films by high-pressure oxygen annealing. J Mater Chem C, 2015, 3(14), 3438

[75] Gao M, Feng D, Yao G, et al. Chemical and mechanical strains tuned dielectric properties in Zr-doped $CaCu_3Ti_4O_{12}$ highly epitaxial thin films. Rsc Adv, 2015, 5(113), 92958

[76] Xie C, Shi L, Zhou S, et al. Structural characteristics, magnetic properties of Re_2NiMnO_6 (Re = La, Pr, Nd, Sm, Y) thin films on (001) $LaAlO_3$ by simple polymer assisted deposition. Surf Coat Tech, 2015, 277, 222

[77] Yao D, Shi L, Zhou S, et al. Tuning the metal–insulator transition via epitaxial strain and Co doping in $NdNiO_3$ thin films grown by polymer-assisted deposition. J Appl Phys, 2016, 119(3), 035303

[78] Chuai Y, Wang X, Zheng C, et al. Highly infrared-transparent and p-type conductive $CuSc_{(1-x)}Sn_{(x)}O_2$ thin films and a p-$CuScO_2$:Sn/n-ZnO heterojunction fabricated by the polymer-assisted deposition method. Rsc Adv, 2016, 6(38), 31726

[79] Lei M, Zhang Y, Zhao Y. Coating conditions of SCO single buffer layer via Slot-Die technique. IEEE T Appl Supercon, 2016, 26(3), 1

[80] Lucas I, Jiménez-Cavero P, Vila-Fungueiriño J M, et al. Chemical solution synthesis and ferromagnetic resonance of epitaxial thin films of yttrium iron garnet. Phys Rev Mater, 2017, 1(7), 074407

[81] Scott B L, Joyce J J, Durakiewicz T D, et al. High quality epitaxial thin films of actinide oxides, carbides, and nitrides: Advancing understanding of electronic structure of f-element materials. Coordin Chem Rev, 2014, 266, 137

[82] Jilek R E, Bauer E, Burrell A K, et al. Preparation of epitaxial uranium dicarbide thin films by polymer-assisted deposition. Chem Mater, 2013, 25(21), 4373

[83] Elbaz L, Kreller C R, Henson N J, et al. Electrocatalysis of oxygen reduction with platinum supported on molybdenum carbide-carbon composite. J Electroanal Chem, 2014, 720, 34

[84] Cobas R, Muñoz-Perez S, Cadogan J M, et al. Magnetoresistance in epitaxial thin films of $La_{0.85}Ag_{0.15}MnO_3$ produced by polymer assisted deposition. Appl Phys Lett, 2011, 99(8), 083113

[85] Kim Y Y, Hwang J S, Kim J K, et al. Electrical and optical properties of hydrogen plasma treated molybdenum doped indium oxide films synthesized by polymer-assisted deposition method. Ceram Int, 2017, 43, S506

[86] Yi Q, Wu J, Zhao J, et al. Tuning bandgap of p-type $Cu_2Zn(Sn, Ge)(S, Se)_4$ semiconductor thin films via aqueous polymer-assisted deposition. ACS Appl Mater Inter, 2017, 9(2), 1602

[87] Hong S J, Jun H, Lee J S. Nanocrystalline WO_3 film with high photo-electrochemical activity prepared by polymer-assisted direct deposition. Scripta Mater, 2010, 63(7), 757

[88] Luo H, Lin Y, Wang H, et al. Amorphous silica nanoparticles embedded in epitaxial $SrTiO_3$ and $CoFe_2O_4$ matrices. Angew Chem Int Edit, 2008, 47(31), 5768

[89] Burrell A K, McCleskey T M, Shukla P, et al. Controlling oxidation states in uranium oxides through epitaxial stabilization. Adv Mater, 2007, 19(21), 3559

[90] Vishwanath S K, An T, Jin W Y, et al. The optoelectronic properties of tungsten-doped indium oxide thin films prepared by polymer-assisted solution processing for use in organic solar cells. J Mater Chem C, 2017, 5(39), 10295

[91] Hwang J S, Lee J M, Vishwanath S K, et al. Effects of H_2 plasma treatment on the electrical properties of titanium-doped indium oxide films prepared by polymer-assisted deposition. J Vac Sci Technol A, 2015, 33(4), 041402

[92] Tao L, Chen K, Chen Z, et al. Centimeter-scale CVD growth of highly crystalline single-layer MoS_2 film with spatial homogeneity and the visualization of grain boundaries. ACS Appl Mater Inter, 2017, 9(13), 12073

[93] Jurca T, Moody M J, Henning A, et al. Low-temperature atomic layer deposition of MoS_2 films. Angew Chem Int Edit, 2017, 56(18), 4991

[94] Shi Y, Zhou Y, Yang D R, et al. Energy level engineering of MoS_2 by transition-metal doping for accelerating hydrogen evolution reaction. J Am Chem Soc, 2017, 139(43), 15479

[95] Suh J, Tan T L, Zhao W, et al. Reconfiguring crystal and electronic structures of MoS_2 by substitutional doping. Nat Commun, 2018, 9(1), 199

[96] Tan H, Hu W, Wang C, et al. Intrinsic ferromagnetism in Mn-substituted MoS_2 nanosheets achieved by supercritical hydrothermal reaction. Small, 2017, 13(39), 1701389

[97] Xiang Z, Zhang Z, Xu X, et al. Room-temperature ferromagnetism in Co doped MoS_2 sheets. Phys Chem Chem Phys, 2015, 17(24), 15822

[98] Cheng Y C, Zhu Z Y, Mi W B, et al. Prediction of two-dimensional diluted magnetic semiconductors: Doped monolayer MoS_2 systems. Phys Rev B, 2013, 87(10), 100401

[99] Liu G, Robertson A W, Li M M, et al. MoS_2 monolayer catalyst doped with isolated Co atoms for the hydrodeoxygenation reaction. Nat Chem, 2017, 9(8), 810

[100] Li B, Xing T, Zhong M Z, et al. A two-dimensional Fe-doped SnS_2 magnetic semiconductor. Nat Commun, 2017, 8, 1958